

## PARTICLE ACCELERATION AT SHOCKS MOVING THROUGH AN IRREGULAR MAGNETIC FIELD

JOE GIACALONE

Department of Planetary Sciences, University of Arizona, 1629 East University Boulevard, Tucson, AZ 85721-0092

Received 2004 August 14; accepted 2005 January 29

### ABSTRACT

We use nondiffusive, nonrelativistic, test-particle numerical simulations to address the physics of particle acceleration by collisionless shocks. We focus on the importance of the shock normal angle,  $\langle\theta_{Bn}\rangle$ , in determining the energy spectrum of the accelerated particles. For reasonable parameters, we find that the injection velocity is weakly dependent on the mean shock normal angle and that low-energy particles are readily accelerated to high energies irrespective of  $\langle\theta_{Bn}\rangle$ . Our results are applicable for shocks that are nearly planar on scales larger than the coherence scale of the upstream magnetic turbulence and for particles whose gyroradii are smaller than this scale. We confirm previous results showing that the acceleration rate is larger for nearly perpendicular shocks compared to parallel shocks. However, we also find that the acceleration rate at parallel shocks moving through large-scale magnetic fluctuations is larger than that predicted by simple first-order Fermi acceleration. Our results can be understood in terms of the nature of the large-scale fluctuations and their effect on particle transport.

*Subject headings:* acceleration of particles — cosmic rays — methods: numerical — shock waves

### 1. BACKGROUND

An essential goal of plasma astrophysics is to understand how charged particles are accelerated in the ionized gases of space. One mechanism in particular, acceleration by collisionless shock waves, has received much recent attention and is the focus of this paper. In the late 1970s, four independent groups were the first to demonstrate the essential physics of diffusive shock acceleration (Krymsky 1977; Axford et al. 1978; Bell 1978; Blandford & Ostriker 1978). They showed that the energy spectrum of particles behind the shock falls off with energy as a universal power law. It is widely accepted that this theory explains the observed cosmic-ray spectrum up to about  $10^{15}$  eV (Blandford & Eichler 1987). A nice review of the subject, including more recent numerical calculations and observations, is given by Jones & Ellison (1991).

Under closer scrutiny, however, the standard theory of diffusive shock acceleration does not obviously explain all phenomena associated with particle acceleration at shocks. In some cases, such as the existence of non-power-law energy spectra, the theory needs only to include losses, or time dependence, or more complicated geometries, in order to explain the observations. However, there is clearly one important aspect of particle acceleration by shocks that has not been explained adequately with the standard theory: the well-known injection problem that relates to the question of how low-energy particles are accelerated.

The injection problem has received considerable attention over the past two decades. Ellison (1981) used a nonlinear Monte Carlo approach and showed that high-energy particles originate from the thermal population incident on quasi-parallel shocks (those that propagate in nearly the same direction as the magnetic field). This work demonstrated that such shocks efficiently accelerate a fraction of the incident plasma and that high-energy particles are intimately coupled to the global shock dynamics (energy dissipation, jump conditions, etc.). Quest (1988), Scholer (1990), and Giacalone et al. (1992) confirmed these results using self-consistent plasma simulations that better treat the physics of wave-particle interactions. The simulations also revealed much about the mechanism involved in the acceleration of thermal particles to high energies (see also Kucharek & Scholer 1991).

Recent theoretical insight has also been gained (Sugiyama et al. 2001).

The acceleration of low-energy particles at quasi-perpendicular shocks, in contrast, has been much more difficult to understand. Because particles must remain near the shock to be efficiently accelerated, the geometry of a nearly perpendicular shock requires efficient cross-field transport. Unfortunately, this process is not fully understood. Using a specific form of the cross-field diffusion coefficient, Baring et al. (1994) and Ellison et al. (1995) showed that the acceleration efficiency for particles accelerated at oblique shocks decreases sharply with increasing shock normal angle. Giacalone & Ellison (2000) and Giacalone (2003) performed hybrid simulations of quasi-perpendicular shocks, but concluded that this type of model is probably not suitable (at present) because computational limitations restrict the size of the (fully three-dimensional) spatial domain to scales much smaller than the observed coherence scale of turbulent magnetic fields in most astrophysical plasmas.

Recent advances in our understanding of cross-field diffusion has motivated the present study. One issue, in particular, has arisen in the past decade: in order to properly study cross-field diffusion, a fully three-dimensional magnetic field must be used (Jokipii et al. 1993; Jones et al. 1998). In addition, it was recently shown by Giacalone & Jokipii (1999) that the ratio of the perpendicular to parallel diffusion coefficient is independent of energy for situations in which the particle gyroradii are smaller than the coherence scale of the magnetic fluctuations. This has important consequences for particle acceleration at perpendicular shocks.

It is the purpose of this paper to examine the importance of the angle between the mean magnetic field vector and the unit shock normal,  $\langle\theta_{Bn}\rangle$ , on the energy spectrum of shock-accelerated particles. This work is an extension of our previous studies (Giacalone & Jokipii 1996; Giacalone & Ellison 2000) covering a broader range of shock normal angles, both time-dependent and steady state particle distributions, and a larger coherence scale for the magnetic fluctuations. The results from our current study reveal new insights into particle acceleration at shocks that were not realized in the previous studies. Our study also adds additional insight into understanding the well-known injection

problem discussed above; however, we note that the particles considered in this study have a minimum energy that is still much higher than that of the thermal distribution. Thus, while we address the acceleration of low-energy particles, the question of how thermal particles are accelerated to high energies is not strictly answered in this study. In order to address this adequately, a self-consistent approach is necessary. However, insufficient computational resources do not presently permit an accurate treatment of this problem, as was discussed in Giacalone & Ellison (2000).

## 2. NUMERICAL MODELS

Our approach is to use a brute force numerical integration of the equations of motion of an ensemble of test particles. Such a method better treats nondiffusive effects that are important with regard to the acceleration of low-energy particles. For most of the simulations performed in this study, we use prespecified magnetic and electric fields. This approach best treats the physics of the important wave-particle interactions. Our model is similar to that of Decker & Vlahos (1986), except that here we consider fully three-dimensional magnetic and electric fields that are required (by theory) to properly treat cross-field diffusion.

### 2.1. Model 1: Large-Scale Magnetic Fluctuations

The numerical model used in this study has been described in detail previously (Giacalone & Jokipii 1996; Giacalone & Ellison 2000). Here we describe the salient details of the model for completeness. We refer the interested reader to the previous papers for a more complete description.

We consider the geometry illustrated in Figure 1. A planar shock is located at  $x = 0$ , and plasma flows in the positive  $x$ -direction in the shock rest frame, with a speed  $U_1$  for  $x \ll 0$  (upstream). In this study, we restrict attention to nonrelativistic flows so that  $U_1 \ll c$ , where  $c$  is the speed of light. The flow decreases downstream of the shock ( $x \gg 0$ ) to a speed  $U_2$ . The flow speed varies smoothly across according to a hyperbolic tangent function with a width  $0.1U_1/\Omega_p$  ( $\Omega_p$  is the proton cyclotron frequency), which is much smaller than the gyroradii of the particles of interest in this study. For all shocks considered in this paper, we take the strong shock limit in which  $U_1/U_2 = 4$ , corresponding to the case where the upstream magnetosonic Mach number,  $M_{ms} \gg 1$ . For the same approximation, it can be readily demonstrated that the downstream flow velocity is also in the positive  $x$ -direction. In addition, effects on the local shock jump conditions due to variations in the local shock normal angle, arising from the convection of large-scale magnetic fluctuations across the shock, can also be neglected in the high Mach limit (Decker 1988). The average magnetic field on either side of the shock,  $\langle \mathbf{B}_{1,2} \rangle$ , lies in the  $x - z$  plane, as indicated in Figure 1. The total magnetic field is  $\mathbf{B}_{1,2} = \langle \mathbf{B}_{1,2} \rangle + \delta \mathbf{B}_{1,2}$ , where  $\delta \mathbf{B}_{1,2}$  is a random magnetic field having a zero mean. The method we use to generate the random field is described in detail in our previous papers (referenced above) and involves an assumed power spectrum (see below). It satisfies Maxwell's equations. Proper boundary conditions are ensured by conserving the transverse components of the electric field and the normal component of the magnetic field across the shock. Note that the transverse magnetic field is compressed by a factor of 4 at the shock. Finally, the motional electric field, in the shock rest frame, is obtained from the usual ideal MHD expression indicated in Figure 1.

For all studies in this paper we assume a power spectrum for the random magnetic field fluctuations of the form

$$P(\mathbf{k}) \propto \frac{1}{1 + (|\mathbf{k}|L_c)^\gamma}, \quad (1)$$

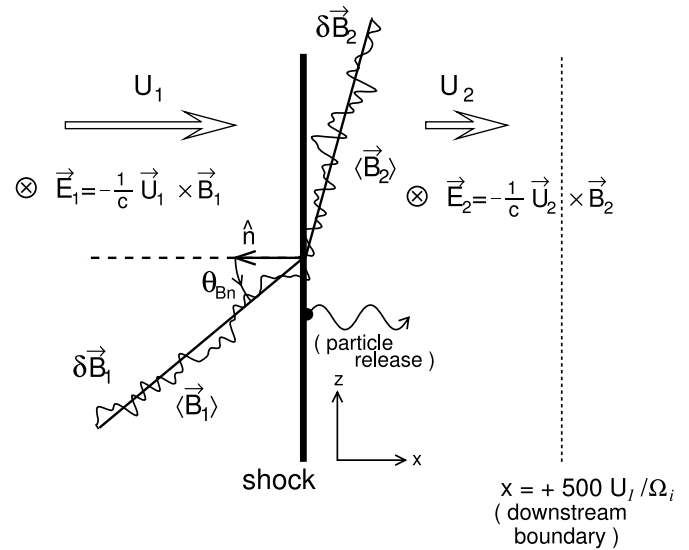


FIG. 1.—Geometry used for all numerical simulations in this study.

where  $\mathbf{k}$  is the wavevector,  $L_c$  is the correlation length of the magnetic fluctuations, and  $\gamma$  is the spectral index. We assume purely isotropic magnetic fluctuations (Batchelor 1960). We also take the correlation length to be  $L_c = 2000U_1/\Omega_p$ , which is much larger than the gyroradii of particles at the injection energy that we consider in this study. It is also larger than the gyroradii of the particles at the maximum energy in all but one of our simulations.

Cross-field diffusion is naturally included in this model and is important for particle acceleration at quasi-perpendicular shocks. Our assumed magnetic field is fully three-dimensional, thereby overcoming the limitations that are artificially imposed on the particle motion in fields that use lesser spatial dimensions, as discussed by Jokipii et al. (1993) and Jones et al. (1998). For large-scale fluctuations with  $L_c \gg r_g$  (where  $r_g$  is the particle gyroradius), as considered in this paper, particles move across the mean field by following along meandering magnetic lines of force, as well as moving across the local magnetic field (e.g., Jokipii 1966; Goldstein et al. 1975; Forman et al. 1974; Giacalone & Jokipii 1999). Using similar turbulence spectra, Giacalone & Jokipii (1999) computed diffusion coefficients from the motion of test particles having various energies. They found that the ratio of the perpendicular to parallel diffusion coefficients are independent of energy over a very broad energy range. They also found that the parallel diffusion coefficient agreed well with the prediction from the quasi-linear theory (e.g., Jokipii 1966). We note that in many simulations used in this study, we vary the mean field direction to obtain different shock normal angles, but we use the same upstream turbulence spectra for the random component. Thus, the perpendicular and parallel diffusion coefficients do not depend on the shock normal angle.

### 2.2. Model 2: Classical Scattering

For the purpose of comparison, we also perform two numerical simulations for the case of classical scattering. This type of model is very similar to those performed by Baring et al. (1994) and Ellison et al. (1995), except that here we assume that the particles do not influence the shock structure (these authors included the back-reaction of the particles on the shock). In this model, the large-scale fluctuations are removed, and the effect of the small scales are mimicked by introducing a phenomenological scattering

law. This gives rise to a different form for the cross-field diffusion coefficient  $\kappa_{\perp}$ . In this case,  $\kappa_{\perp}$  is given by the usual hard sphere scattering result (e.g., Chapman & Cowling 1970; Parker 1965; Forman & Gleeson 1975).

In order to compare with the simulations in which the large-scale fluctuations are present, we consider the case in which the parallel mean free paths obtained from the two models are the same. It was shown by Giacalone & Jokipii (1999) that the parallel diffusion coefficient determined from the quasi-linear theory nicely agrees with that determined from numerical simulations involving large-scale fluctuations. Thus, we can determine a scattering law from the quasi-linear theory (Jokipii 1966; Earl 1974; Luhmann 1976) for our assumed power spectrum. The same form for the power spectrum was used by Giacalone & Jokipii (1999), who derived a formula for the parallel diffusion coefficient,  $\kappa_{\parallel}$  (see the Appendix in their paper). Using this formula and  $\lambda_{\parallel} = 3\kappa_{\parallel}/w$ , where  $w$  is the particle speed, we find

$$\lambda_{\parallel} \simeq 4.9 \left( \frac{B}{\Delta B} \right)^2 \left( \frac{\Omega_p L_c}{w} \right)^{2/3} r_g, \quad (2)$$

where  $r_g = w/\Omega_p$  is the particle gyroradius. Taking  $\Delta B = B$  and  $L_c = 2000U_1/\Omega_p$ , we find

$$\frac{\lambda_{\parallel}}{r_g} \simeq 530 \left( \frac{w}{w_0} \right)^{-2/3}, \quad (3)$$

where  $w_0 = \sqrt{3}U_1$  is the initial particle speed (see § 2.3).

Note that the mean free path in these fluctuations is quite large. This is due to the fact that most of the power resides in the long-wavelength modes, and there is very little power at the resonant scale (which determines  $\lambda_{\parallel}$  in the quasi-linear theory).

For this model, the particles are scattered phenomenologically by determining a scattering time based on an exponential distribution with a mean scattering time  $\tau$ , which is related to the scattering mean free path derived in equation (3). The particles are scattered isotropically in the local plasma frame of reference.

### 2.3. Test Particles

We assume that the particles (protons) have a negligible effect on the shock fields and microstructure and can be considered test particles. The back-reaction of the particles on the fields may be important (e.g., Ellison & Eichler 1984), but this effect is difficult to model for our case involving prespecified magnetic field fluctuations. We also consider particles that have larger gyroradii than the width of the shock, which is of the order of a few thermal proton gyroradii (e.g., Winske 1985). We therefore neglect such aspects of the shock microstructure as the magnetic overshoot (Giacalone et al. 1991), cross-shock electric field (Zank et al. 1996; Lee et al. 1996; Rice et al. 2000), and the noncoplanar magnetic fields (e.g., Gosling et al. 1988).

We numerically integrate the orbits of 100,000 test particles. The initial position of each particle is  $x = 0$  (at the shock) and has an initial velocity vector that is determined from an isotropic distribution in the local plasma frame having a total speed  $w_0 = \sqrt{3}U_1$ . Each particle moves under the influence of the magnetic and electric forces described above, and each is given a different random magnetic field realization (see Giacalone & Jokipii 1996 for details). The nonrelativistic equations of motion for each particle are numerically integrated forward in time using the Burlirsh-Stoer method (Press et al. 1986). The algorithm uses an adjustable time step based on an evaluation of the local trunca-

tion error. Energy is conserved in our numerical simulations to an accuracy of better than 0.2%. In addition, the statistics in the high-energy portion of the particle distributions are improved by incorporating ‘‘particle splitting,’’ which is a well-known and well-tested method described in our previous papers.

### 2.4. Steady State and Time-Dependent Calculations

We consider both steady state and time-dependent particle distributions.

For the case of steady state calculations, each particle is followed until either it crosses a physical boundary located at  $x = 500U_1/\Omega_p$  or its momentum, measured relative to the local plasma frame, becomes greater than  $500m_pU_1$  (where  $m_p$  is the proton mass). Upon crossing the momentum boundary, the particle is removed from the system. When the particle crosses the spatial boundary, it may be removed from the system depending on whether it passes a ‘‘probability of escape’’ test. This is described in detail in our previous papers. We note that the location of the downstream boundary is shorter than the coherence length of the upstream fluctuations. We have performed additional numerical simulations (not listed in Table 1) in order to test the effect of the location of the downstream boundary. We have found that our results do not change if this boundary is moved farther downstream of the shock.

For the time-dependent case, particles are released at a random time between 0 and  $t_{\max}$ , the maximum simulation time. For all time-dependent simulations that we report in this study, we take  $t_{\max} = 50,000 \Omega_p^{-1}$ . For a typical heliospheric magnetic field at a distance of 10 solar radii (1600 nT), 1 AU (5 nT), and 90 AU (0.04 nT), this time corresponds to 5.4 minutes, 1.2 days, and 0.4 yr, respectively. Each particle is followed until  $t = t_{\max}$ , or it is removed from the system at the downstream boundary in the same manner as described above for the steady state calculations. Note that there is not a momentum boundary for this case.

### 2.5. Summary of Numerical Simulations

We have performed a total of 16 numerical simulations. The key parameters are listed in Table 1. Note that in all simulations, the shock strength (ratio of the upstream to downstream flow speed) is 4. This corresponds to the case of a high Mach shock. Figures 2–5, 7, and 8 all show differential intensity spectra as a function of energy measured downstream of the shock. These spectra were obtained by computing  $dJ/dE = p^2f$ , where  $p$  is the particle momentum and  $f$  is the phase-space distribution function. The spatial region over which the distribution is computed is  $0.25x_{\text{DOWN}} < x < x_{\text{DOWN}}$ , where  $x_{\text{DOWN}}$  is the location of the downstream boundary. Over this region, the distribution is fairly uniform in space.

## 3. RESULTS

Figures 2–5 show results for the case of strong magnetic fluctuations. For this we take the total integrated power in the random component of the magnetic field to be equal to that in the mean. In the next section, we show results (Figs. 7 and 8) of calculations for the case of weaker magnetic turbulence.

In Figure 2, we plot results obtained from five simulations having different values of  $\langle \theta_{Bn} \rangle$ , as indicated. These are simulations 1–5 in Table 1. Note that the curves for  $\langle \theta_{Bn} \rangle = 0^\circ, 15^\circ$ , and  $30^\circ$  are all the same and lie on top of one another. The spectra are obtained for the case of a steady state simulation (described above).

Figure 2 shows that, irrespective of the shock normal angle, particles are readily accelerated from the injection energy to the

TABLE 1  
SUMMARY OF SIMULATIONS

Simulation Number	Model	Type	$\langle\theta_{Bn}\rangle$ (deg)	$(\Delta B/B)^2$
1.....	1 (Magnetic)	Steady state	0	1
2.....	1 (Magnetic)	Steady state	15	1
3.....	1 (Magnetic)	Steady state	30	1
4.....	1 (Magnetic)	Steady state	45	1
5.....	1 (Magnetic)	Steady state	60	1
6.....	1 (Magnetic)	Steady state	75	1
7.....	1 (Magnetic)	Steady state	90	1
8.....	2 (Classical)	Steady state	90	1 <sup>a</sup>
9.....	1 (Magnetic)	Time-dependent	0	1
10.....	1 (Magnetic)	Time-dependent	45	1
11.....	1 (Magnetic)	Time-dependent	90	1
12.....	2 (Classical)	Time-dependent	0	1 <sup>a</sup>
13.....	1 (Magnetic)	Steady state	90	0.3
14.....	1 (Magnetic)	Steady state	90	0.1
15.....	1 (Magnetic)	Time-dependent	0	0.1
16.....	1 (Magnetic)	Time-dependent	90	0.1

<sup>a</sup> In the classical scattering model, actual magnetic turbulence is not used. This is the value used in the quasi-linear theory to determine the mean free path that is used in the classical scattering model (see text for details).

maximum energy allowed. The spectra for the quasi-perpendicular shocks are steeper compared to the quasi-parallel shocks in the energy range of  $100 \lesssim E/E_p \lesssim 10^4$ , where  $E_p = mU_1^2/2$  is the plasma ram energy. All spectra have the same power-law slope for energies beyond  $5 \times 10^4 E_p$  and are consistent with the prediction of diffusive shock acceleration theory. The simulated slope at high energies (in all cases) is  $-0.98 \pm 0.03$ , which is in agreement with the expected strong shock value of  $-1$ . It is not clear to us, at present, what causes the spectral steepening in the energy range  $100 \lesssim E/E_p \lesssim 10^4$  for the quasi-perpendicular shocks.

The results shown in Figure 2 indicate that the injection energy is weakly dependent on the mean shock normal angle. This can be understood in terms of the spatial diffusion tensor associated with the particle motions, as discussed by Giacalone & Jokipii (1999) and Giacalone & Ellison (2000). The large-scale fluctuations increase the diffusion coefficient normal to the mean magnetic field because particles move approximately along meandering lines of force that significantly deviate from the mean field direction. The increased diffusion normal to the field, for the case of a perpendicular shock, leads to a lower injection threshold. We would expect that the diffusion tensor, and its dependence on

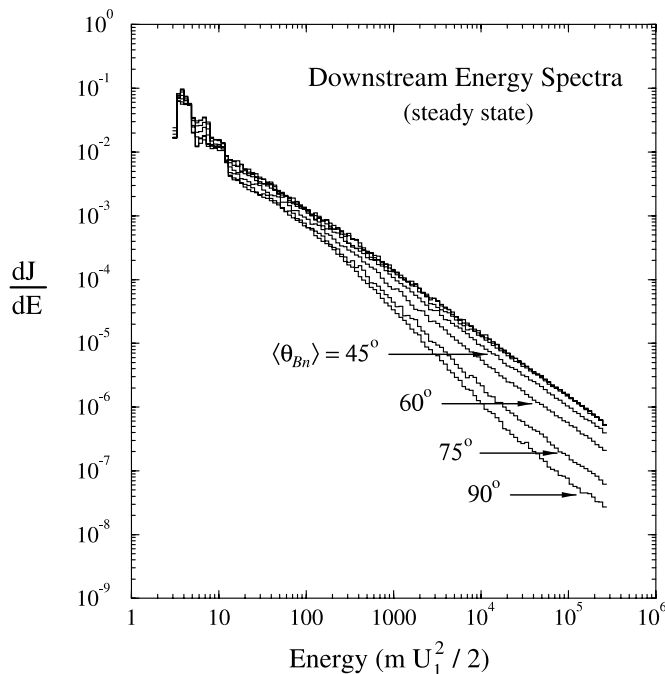


FIG. 2.—Simulated steady state energy spectra, downstream of the shock, as a function of energy for various values of the mean shock normal angle, as indicated. Results from runs 1–7 (see Table 1) are shown.

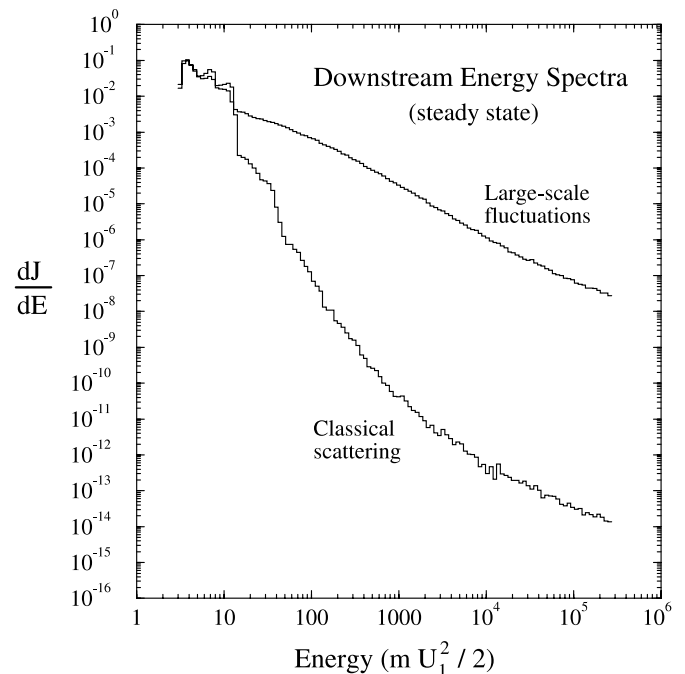


FIG. 3.—Comparison of the downstream, steady state energy spectra from two different models, as indicated, for a perpendicular shock (simulations 7 and 8).

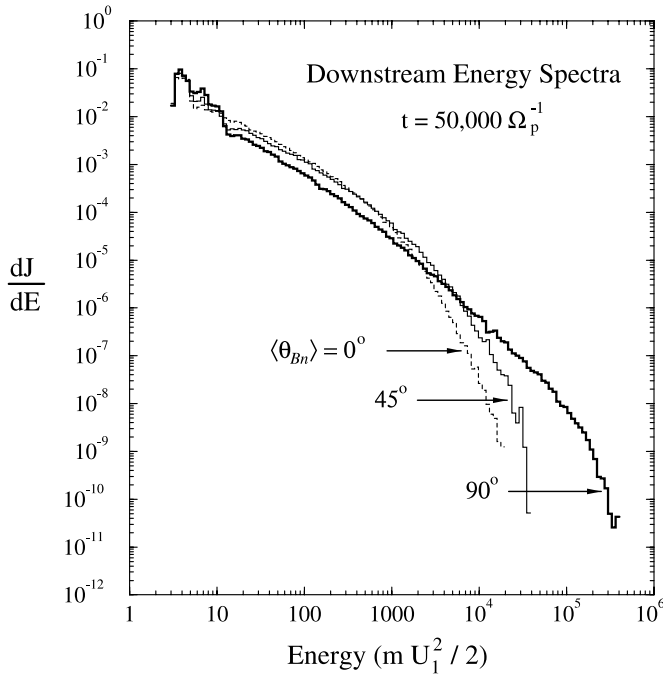


FIG. 4.—Downstream energy spectra at  $t = 50,000 \Omega_p^{-1}$  for three different mean shock normal angles, as indicated. The perpendicular shock accelerates particles to higher energies compared to the parallel shock at the same simulation time. Results from simulations 9–11 are shown.

energy, is important in determining the form of the downstream energy spectrum of shock-accelerated particles at low energies. However, just exactly how is unclear and will be considered in a later study.

Figure 3 shows energy spectra for a perpendicular shock. The upper curve is the same as shown in Figure 2 for  $\langle \theta_{Bn} \rangle = 90^\circ$ . The lower curve was obtained from a different numerical simulation that uses classical scattering, which was described above. These are simulations 7 and 8 in Table 1. The purpose of this figure is to illustrate the importance of the large-scale fluctuations. This influences the form of the diffusion coefficient, which can have a profound effect on the acceleration of low-energy charged particles (Giacomone & Jokipii 1999). This is clearly evident in Figure 3, as the difference in the spectra at the highest energies is more than 6 orders of magnitude. Note that for the case of classical scattering there is strong decrease in the energy spectrum at about  $12E_p$  and another decrease at about  $30E_p$ . These are associated with nondiffusive effects arising from discrete particle-shock interactions. Some particles cross the shock only twice, moving from downstream to upstream, and then back downstream, where they convect away from the shock. Some particles cross the shock only four times, some only six, and so on. Some of these populations can be identified in the distribution for the classical scattering case in which the local shock normal angle never changes. They are not as easily identified in the large-scale fluctuations case because of the large variability in the local shock normal angle.

The spectra shown in Figure 4 were obtained from a time-dependent simulation. These are simulations 9, 10, and 11 in Table 1. The figure shows that, at the same simulation time, the parallel shock accelerates particles to a characteristic energy of about  $1000E_p$ , whereas the perpendicular shock accelerates them to over  $10^5E_p$ . Consequently, the flux at the highest energies is dominated by particles accelerated at the perpendicular shock. This confirms the earlier studies by Jokipii (1982, 1987) and

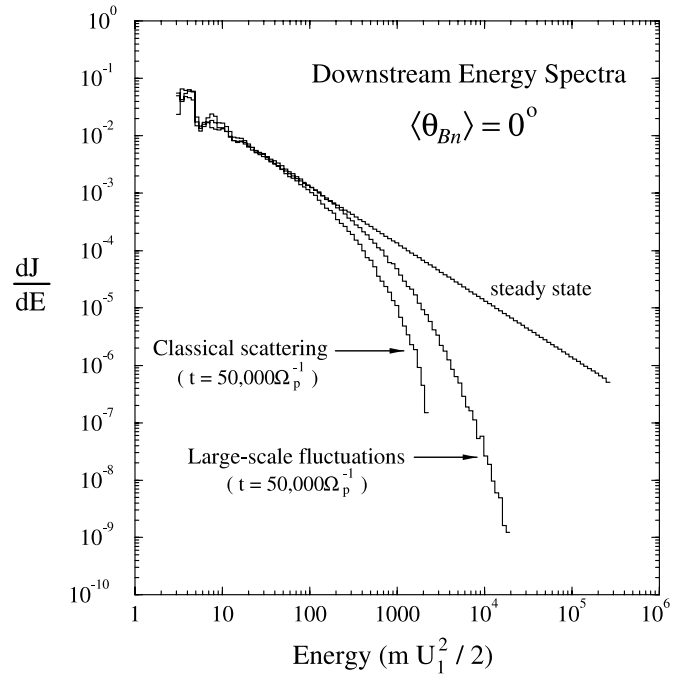


FIG. 5.—Comparison of the downstream, time-dependent energy spectra obtained for particles accelerated by parallel shock. The steady state spectrum is shown for reference. Two different models are shown, as indicated (see text for details). These are simulations 1, 9, and 12.

Ostrowski (1991) showing that perpendicular shocks accelerate particles faster (at a higher rate) than parallel shocks. Note that the spectra shown in Figure 4 turn over (become softer) at high energies because of the time dependence. In contrast, the spectra shown in Figure 2, which are in steady state, become somewhat softer at low energies for the quasi-perpendicular shocks ( $\langle \theta_{Bn} \rangle > 45^\circ$ ) for a different reason. This is probably related to the form of the diffusion coefficient as discussed above.

Figure 5 shows energy spectra for a parallel shock (on average). The two curves that turn over at a characteristic energy are from a time-dependent simulation (as indicated), while the other is for the case of a steady state spectra (also shown in Fig. 1). These are simulations 1, 9, and 12 in Table 1.

We find that the large-scale fluctuations have another important consequence: they lead to a higher acceleration rate at a parallel shock compared to the case of simple first-order Fermi acceleration (the classical scattering case). This is due to the fact that, at times, the local magnetic field is more oblique to the shock normal. Thus, even for a parallel shock (on average), acceleration can occur locally at the shock because of drift acceleration. This is illustrated in Figure 6. The figure shows two plots of a typical energetic particle trajectory for the case of a parallel shock ( $\langle \theta_{Bn} \rangle = 0^\circ$ ). Note that only a segment of the complete trajectory is shown. This particle continued to gain energy and remained in the system much longer than is shown. The left plot is the kinetic energy, measured in the shock frame, as a function of position. The right plot is the kinetic energy as a function of time for the same particle. Note that there is a large gain in energy at the point labeled (d) in both plots that occurs over a short period of time compared to the others (labeled a, b, c, and e). At this part of the orbit, the particle is drifting along the shock. Such an orbit is not possible in the case of classical scattering at a parallel shock since there is no compression of the magnetic field. For the case of large-scale fluctuations, there can be compressions of the total field at the shock due to the presence of the

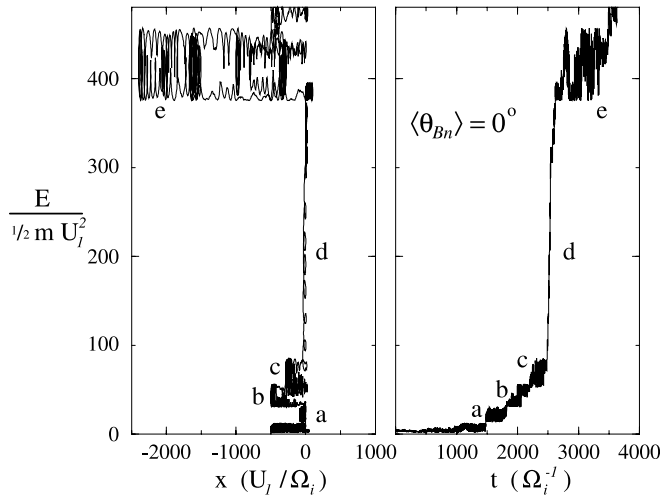


FIG. 6.—Typical individual particle trajectory for the parallel shock case ( $\langle \theta_{Bn} \rangle = 0^\circ$ ). The left panel shows the shock frame energy as a function of position, and the right panel shows the energy as a function of time. The labels a, b, c, d, and e highlight parts of the orbit that are discussed further in the text.

waves (recall that the transverse components of the magnetic field are compressed to ensure the proper boundary conditions).

#### 4. THE EFFECT OF WEAKER MAGNETIC FLUCTUATIONS

We now consider cases in which the total integrated power in the upstream magnetic fluctuations is smaller than that in the mean field. We have performed four additional simulations, which are simulations 13–16 in Table 1.

Figure 7 shows the steady state downstream energy spectra for a perpendicular shock for three different values of  $(\Delta B/B)^2$ . Interestingly, the spectra at high energies are the same for the case of  $(\Delta B/B)^2 = 1$  and  $(\Delta B/B)^2 = 0.3$ . The reason for this is

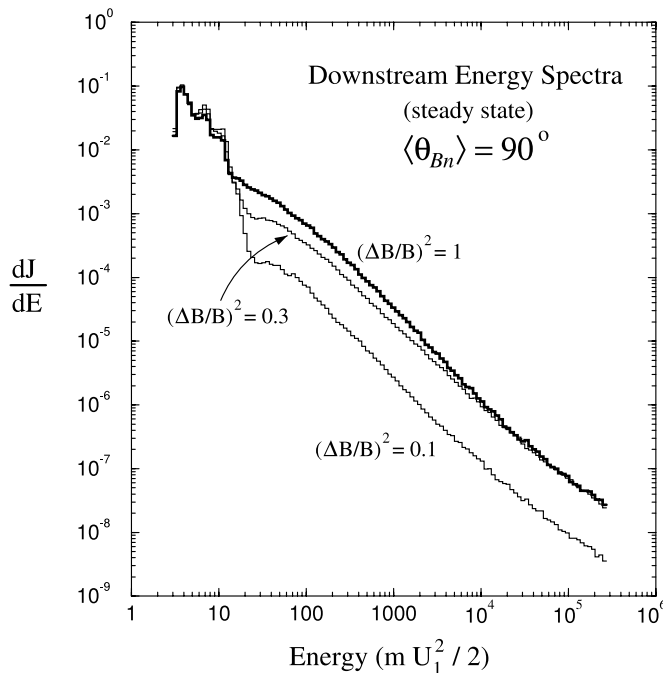


FIG. 7.—Comparison of downstream energy spectra for perpendicular shocks moving through irregular magnetic field fluctuations with varying values for the total integrated power, as indicated (simulations 7, 13, and 14).

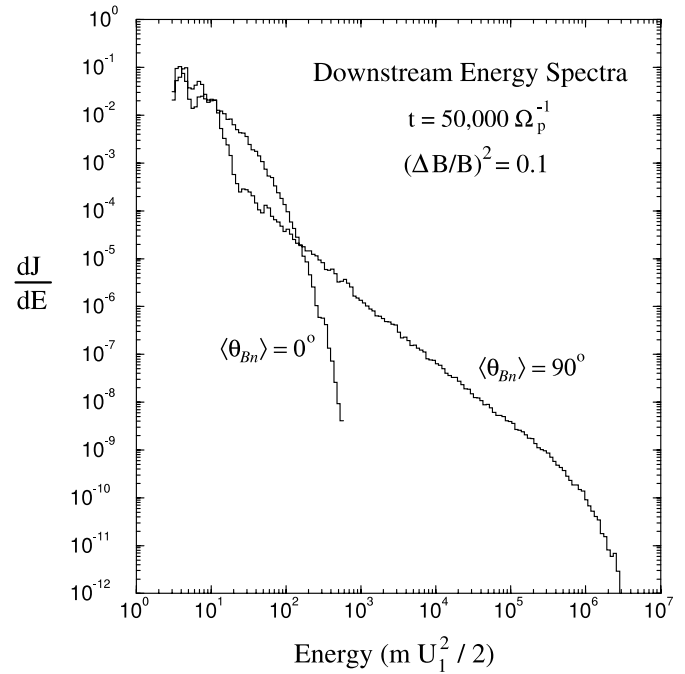


FIG. 8.—Simulated time-dependent downstream energy spectra for both a perpendicular and parallel shock, for the case of weak magnetic fluctuations  $\Delta B/B = 0.1$  (simulations 15 and 16).

not clear at present. Moreover, even for the case of the weakest turbulence that we have studied, the perpendicular shock readily accelerates particles to high energies and there is no injection problem.

Figure 8 shows the time-dependent downstream energy spectra at  $t = 50,000 \Omega_p^{-1}$  for the case of  $(\Delta B/B)^2 = 0.1$  for a parallel and a perpendicular shock. There is a dramatic difference in the maximum energy. For the weak turbulence case, the acceleration rate at a parallel shock is very small because the particle mean free paths are very large (10 times larger than that estimated in eq. [3]). However, the perpendicular shock readily accelerates particles to very high energies because these particles are capable of diffusing normal to the mean magnetic field direction by following meandering magnetic field lines.

#### 5. APPLICATION TO ASTROPHYSICAL SHOCKS

We now consider various astrophysical applications of our numerical simulation results.

##### 5.1. Solar Wind Termination Shock

Anomalous cosmic rays (ACRs) are probably interstellar pickup ions that have been accelerated, at least in part, by the termination shock of the solar wind (Fisk et al. 1974; Pesses et al. 1981). In order to explain the observed charge state of ACRs, Jokipii (1992) showed that the shock must be nearly perpendicular over most of its surface.

The results from our calculations indicate that pickup ions should be readily accelerated locally at the termination shock to ACR energies, provided the magnetic field turbulence in the outer heliosphere is similar to what we have used in our model. Observations reported by Smith et al. (2001) indicate that the coherence scale of the heliospheric magnetic field is  $\sim 0.1$  AU (at 30 AU) and increases rapidly with heliocentric distance. It is reasonable to assume that at 100 AU (near the termination shock) the coherence scale is  $\sim 0.5$ –1 AU. This is the gyroradius of a proton with an energy of  $\sim 0.5$  GeV at that distance, which is

about the same as the highest energy ACRs. Thus, we feel that our model can be directly applied to the physics of the termination shock. Note that we reached a different conclusion in our previous paper (Giacalone & Jokipii 1996; Giacalone et al. 1997), noting that some preacceleration of the pickup ions must occur in the inner heliosphere. The new results indicate that this may not be necessary, but does not rule out this possibility.

### 5.2. Earth's Bow Shock

The results of our study are not directly applicable to the case of energetic particles associated with Earth's bow shock. We have assumed a planar shock on scales larger than the magnetic field coherence scale. The typical scale of Earth's bow shock (tens of Earth radii, or  $\sim 10^5$  km) is much smaller than the coherence scale of the interplanetary magnetic field fluctuations ( $\sim 10^6$  km).

### 5.3. Shocks Associated with Solar Coronal Mass Ejections

Near the Sun, the coherence scale of the magnetic fluctuations is probably of the order of the solar radius, and the amplitude is fairly weak, as inferred from density scintillation observations (Spangler 2002). At 5 solar radii, the correlation length is much larger than the gyroradii of even tens of GeV particles, which are the highest energy particles the Sun is known to produce. Moreover, the radius of curvature of shocks associated with a coronal mass ejections (CMEs) is also, reasonably, of this order. Thus, our results should be applicable to understanding the origin of the high-energy solar cosmic rays associated with gradual solar flare events (Reames 1999).

Our results indicate that the highest energy particles ( $\gtrsim 100$  MeV) originate from regions of the CME shock such that the unit normal is nearly perpendicular to the magnetic field. Perpendicular shocks exist at the flanks of CMEs, where the shock is expanding across open solar magnetic field lines. They may also exist nearer the Sun, where shocks (or compressions) are formed because of the release of energy associated with the reconfiguration of magnetic fields there. Parallel shocks moving into regions containing only the ambient magnetic fluctuations clearly do not have enough time to accelerate particles to these energies (see Fig. 8). However, we have not considered here the effect of added magnetic fluctuations arising from the excitation of waves by the energetic particles themselves (Lee & Ryan 1986; Zank et al. 2000; Rice et al. 2003; Li et al. 2003).

### 5.4. Supernova Remnants

Our calculations may also be applicable to our understanding of variations of cosmic-ray intensity inferred from synchrotron emission from supernova remnants. A typical coherence scale of the interstellar magnetic field is about 2 pc, which is the gyroradius of an  $\sim 5 \times 10^{15}$  eV proton in a 3  $\mu$ G field (typical of the interstellar field). This energy is of the same order as that believed to be the maximum energy of cosmic rays accelerated

by supernova remnants. We must also consider the size of the shock. As in the case of the Earth's bow shock (above), our results are applicable only if the shock can be considered to be planar on scales larger than the magnetic field turbulence coherence length. For a supernova shock moving at a speed of, for example, 3000 km s<sup>-1</sup>, it would take about 600 yr for the shock to have a radius equal to the interstellar magnetic field coherence length. Thus, our results may be applicable to fairly old supernova remnants. However, because our simulations are for non-relativistic particle energies and shock speeds, our results are only strictly applicable for very low energy cosmic rays.

Our calculations indicate that the injection of cosmic rays over the surface of a supernova remnant should be fairly uniform. This is in contrast to the results from Völk et al. (2003). However, as can be seen in Figure 2, given a long enough time to accelerate the particles, the parallel shock is somewhat more efficient at accelerating particles compared to the perpendicular shock. Thus, perhaps variations of a factor of 10 can be explained with the results from our calculations and would favor the view that the observed anisotropy of synchrotron emission (Kesteven & Caswell 1987) is due to more efficient acceleration at the regions where the shock normal is parallel to the interstellar field. However, this cannot be confirmed until direct, fully relativistic simulations of a supernova remnant, using realistic parameters, are performed.

## 6. DISCUSSION AND SUMMARY

We have used numerical simulations of test particles accelerated by collisionless shocks moving into a medium containing a large-scale irregular magnetic field to study the effect of the mean shock normal angle on the resulting energy spectrum of the accelerated particles. Our primary conclusion is that for reasonable magnetic turbulence and shock parameters, the injection velocity is weakly dependent on shock normal angle. Low-energy particles (as low as 3 times the upstream plasma flow energy) are efficiently accelerated to high energies irrespective of the shock normal angle. We also find that the large-scale magnetic field fluctuations have other important effects on the accelerated particle spectra. On one hand, it is clear that perpendicular shocks accelerate particles at a higher rate compared to parallel shocks, confirming earlier studies (Jokipii 1982, 1987; Ostrowski 1991). On the other hand, our simulations indicate that the acceleration rate at parallel shocks is larger than predicted from simple first-order Fermi acceleration.

I gratefully acknowledge Randy Jokipii, Jozsef Kóta, and Rob Decker for useful discussions related to this study. This work was supported in part by NASA under grants NAG5-7793 (Sun-Earth-Connection Guest Investigator Program) and NAG5-12919 (Solar & Heliospheric SR&T Program) and by NSF under grant ATM-0327773 (SHINE program).

## REFERENCES

- Axford, W. I., Leer, E., & Skadron, G. 1978, Proc. 15th Int. Cosmic-Ray Conf. (Plovdiv), 132  
 Baring, M. G., Ellison, D. C., & Jones, F. C. 1994, ApJS, 90, 547  
 Batchelor, G. K. 1960, The Theory of Homogeneous Turbulence (Cambridge: Cambridge Univ. Press)  
 Bell, A. R. 1978, MNRAS, 182, 147  
 Blandford, R. D., & Eichler, D. 1987, Phys. Rep., 154, 1  
 Blandford, R. D., & Ostriker, J. P. 1978, ApJ, 221, L29  
 Chapman, S., & Cowling, T. G. 1970, The Mathematical Theory of Non-Uniform Gases (3rd ed.; Cambridge: Cambridge Univ. Press)  
 Decker, R. B. 1988, Space Sci. Rev., 48, 195  
 Decker, R. B., & Vlahos, L. 1986, ApJ, 306, 710  
 Earl, J. A. 1974, ApJ, 193, 231  
 Ellison, D. C. 1981, Geophys. Res. Lett., 8, 991  
 Ellison, D. C., Baring, M. G., & Jones, F. C. 1995, ApJ, 453, 873  
 Ellison, D. C., & Eichler, D. 1984, ApJ, 286, 691  
 Fisk, L. A., Koslovsky, B., & Ramaty, R. 1974, ApJ, 190, L35  
 Forman, M. A., & Gleeson, L. J. 1975, Ap&SS, 32, 77  
 Forman, M. A., Jokipii, J. R., & Owens, A. J. 1974, ApJ, 192, 535  
 Giacalone, J. 2003, Planet. Space Sci., 51, 659

- Giacalone, J., Armstrong, T. P., & Decker, R. B. 1991, *J. Geophys. Res.*, 96, 3621
- Giacalone, J., Burgess, D., Schwartz, S. J., & Ellison, D. C. 1992, *Geophys. Res. Lett.*, 19, 433
- Giacalone, J., & Ellison, D. C. 2000, *J. Geophys. Res.*, 105, 12541
- Giacalone, J., & Jokipii, J. R. 1996, *J. Geophys. Res.*, 101, 11095
- . 1999, *ApJ*, 520, 204
- Giacalone, J., Jokipii, J. R., Decker, R. B., Krimigis, S. M., Scholer, M., & Kucharek, H. 1997, *ApJ*, 486, 471
- Goldstein, M. A., Klimas, A. J., & Sandri, G. 1975, *ApJ*, 195, 787
- Gosling, J. T., Winske, D., & Thomsen, M. F. 1988, *J. Geophys. Res.*, 93, 2735
- Jokipii, J. R. 1966, *ApJ*, 146, 480
- . 1982, *ApJ*, 255, 716
- . 1987, *ApJ*, 313, 842
- . 1992, *ApJ*, 393, L41
- Jokipii, J. R., Kóta, J., & Giacalone, J. 1993, *Geophys. Res. Lett.*, 20, 1759
- Jones, F. C., & Ellison, D. C. 1991, *Space Sci. Rev.*, 58, 259
- Jones, F. C., Jokipii, J. R., & Baring, M. G. 1998, *ApJ*, 509, 238
- Kesteven, M. J., & Caswell, J. L. 1987, *A&A*, 183, 118
- Krymsky, G. F. 1977, *Dokl. Akad. Nauk SSSR*, 234, 1306
- Kucharek, H., & Scholer, M. 1991, *J. Geophys. Res.*, 96, 21195
- Lee, M. A., & Ryan, J. M. 1986, *ApJ*, 303, 829
- Lee, M. A., Shapiro, V. D., & Sagdeev, R. Z. 1996, *J. Geophys. Res.*, 101, 4777
- Li, G., Zank, G. P., & Rice, W. K. M. 2003, *J. Geophys. Res.*, 108, SSH 10-1
- Luhmann, J. G. 1976, *J. Geophys. Res.*, 81, 2089
- Ostrowski, M. 1991, *MNRAS*, 249, 551
- Parker, E. N. 1965, *Planet. Space Sci.*, 13, 9
- Pesses, M. E., Jokipii, J. R., & Eichler, D. 1981, *ApJ*, 246, L85
- Press, W. H., Flannery, B. P., Teukolsky, S. A., & Vetterling, W. T. 1986, *Numerical Recipes in FORTRAN* (Cambridge: Cambridge Univ. Press)
- Quest, K. B. 1988, *J. Geophys. Res.*, 93, 9649
- Reames, D. V. 1999, *Space Sci. Rev.*, 90, 413
- Rice, W. K. M., Zank, G. P., & le Roux, J. A. 2000, *Geophys. Res. Lett.*, 27, 3793
- Rice, W. K. M., Zank, G. P., & Li, G. 2003, *J. Geophys. Res.*, 108, SSH 5-1
- Scholer, M. 1990, *Geophys. Res. Lett.*, 17, 1821
- Smith, C. W., Matthaeus, W. H., Zank, G. P., Ness, N. F., Oughton, S., & Richardson, J. D. 2001, *J. Geophys. Res.*, 106, 8253
- Spangler, S. R. 2002, *ApJ*, 576, 997
- Sugiyama, T., Fujimoto, M., & Mukai, T. 2001, *J. Geophys. Res.*, 106, 21657
- Völk, H. J., Berezhko, E. G., & Ksenofontov, L. T. 2003, *A&A*, 409, 563
- Winske, D. 1985, in *Collisionless Shocks in the Heliosphere: Review of Current Research*, ed. B. T. Tsurutani & R. G. Stone (Washington: AGU), 225
- Zank, G. P., Pauls, H. L., Cairns, I. H., & Webb, G. M. 1996, *J. Geophys. Res.*, 101, 457
- Zank, G. P., Rice, W. K. M., & Wu, C. C. 2000, *J. Geophys. Res.*, 105, 25079